Faraday Discussions

Template Assisted Lithium Superoxide Growth for Lithium-Oxygen Batteries

Journal:	*Faraday Discussions*
Manuscript ID	FD-ART-06-2023-000116.R2
Article Type:	Paper
Date Submitted by the Author:	21-Jul-2023
Complete List of Authors:	Wang, Hsien-Hau; Argonne National Laboratory, Zhang, Chengji; University of Illinois Chicago, Mechanical Engineering Gao, Jing; Argonne National Laboratory Lau, Kah Chun ; California State University, Physics and Astronomy; Cal State Univ Northridge Plunkett, Samuel; Nivalis Energy System Park, Moon; Argonne National Laboratory, Materials Science Division Amine, Rachid; University of Illinois at Chicago, Chemical Engineering; Argonne National Laboratory, Materials Science Division Curtiss, Larry; Argonne National Laboratory,

Template Assisted Lithium Superoxide Growth for Lithium-Oxygen Batteries

Hsien-Hau Wang,[1] Chengji Zhang,[1,2] Jing Gao,[1,2] Kah Chun Lau,[1,3] Samuel T. Plunkett,[1,2] Moon Park,[1] Rachid Amine,[1] and Larry A. Curtiss[1]

[1]*Materials Science Division, Argonne National Laboratory, Lemont, IL, USA*

[2]*Department of Chemical Engineering, University of Illinois at Chicago, Chicago, IL, USA*

[3]*Department of Physics and Astronomy, California State University, Northridge, CA, USA*

hauwang@anl.gov, (630) 252-3461

Abstract

Developing batteries with energy densities comparable to internal combustion technology is essential for a worldwide transition to electrified transportation. Li-O_2 batteries are seen as the 'holy grail' of battery technologies since they have the highest theoretical energy density of all battery technologies. Current lithium-oxygen (Li-O_2) batteries suffer from large charge overpotentials related to electronic resistivity of the insulating lithium peroxide (Li_2O_2) discharge product. One potential solution is the formation and stabilization of a lithium superoxide (LiO_2) discharge intermediate that exhibits good electronic conductivity. However, LiO_2 is reported to be unstable at ambient temperature despite its favorable formation energy at -1.0 eV/atom. In this paper, based on our recent work on the development of cathode materials for aprotic lithium oxygen batteries including two intermetallic compounds, $LiIr_3$ and LiIr, that are found to form good template interfaces with LiO_2, a simple goodness of fit R factor to gauge how well a template surface structure can support LiO_2 growth is developed. The R factor is a quantitative measurement to calculate the geometric difference in the unit cells of specific Miller Index 2D planes of the template surface and LiO_2. Using this as a guide, the R factors for $LiIr_3$, LiIr, and $La_2NiO_{4+\delta}$, are found to be good. This guide is attested by simple extension to other noble metal intermetallics with electrochemical cycling data including $LiRh_3$, LiRh, and Li_2Pd. Finally, the template concept is extended to main group elements and the R factors for LiO_2 (111) and Li_2Ca suggest that Li_2Ca is a possible candidate for the template assisted LiO_2 growth strategy.

Introduction

Due to global warming, increasing extreme weather and non-sustainable fossil fuel, society is moving toward renewable energy sources and new energy storage systems. Lithium-oxygen/air batteries have a very high theoretical energy capacity approaching 3500 Wh/Kg that is close to gasoline and has attracted much research interest.[1] Despite the promising goal, some hurdles toward applications include: 1) High over-potential during charge and the resulting large over-potential gap; 2) Poor electrochemical cycling; and 3) Low charging/discharging rates. These hurdles are not entirely independent. The high overpotential is one of the main reasons for reduced long term cycling stability. The high overpotential is largely caused by the lithium peroxide (Li_2O_2) discharge product. Due to the insulating nature of Li_2O_2, it is difficult for current to pass through upon accumulation on the cathode. To avoid this problem, some research has been on developing new catalysts that lead to lithium superoxide (LiO_2) as the discharge product. LiO_2 has been reported as lithium deficient Li_2O_2 (i.e., $Li_{2-x}O_2$) and early calculations suggested its conductive nature as a semi-metal. [2-4] The theoretical calculations turned out to be very challenging to verify since LiO_2 is not stable at ambient temperatures.[3, 5] To date, to our knowledge, there is no reported experimental single crystal structure, no four-probe conductivity measurement, nor other physical property measurements on isolated pure LiO_2 crystallites. Recent calculations indicate crystalline LiO_2 is still a wide band gap insulator. However, the calculated Li ionic conductivity (4×10^{-9} S/cm at room temperature) and electronic conductivity (9×10^{-12} S/cm at 300 K) are 10 and 8 orders of magnitude larger than that of the Li_2O_2 (4×10^{-19} S/cm and 5×10^{-20} S/cm), respectively. The high ionic and electronic conductivities of LiO_2 are due to a polaron hopping mechanism whereby the induced polarization by the charge in the crystal lattice facilitates the conduction passage.[6] Since the ionic and electronic conductivity of LiO_2 are significantly higher than that of the Li_2O_2, LiO_2 could be a beneficial discharge product for a Li-O_2 cell.

In 2016 a Li-O_2 battery was reported based on Ir nanoparticles prepared through a hydrothermal route for a Ir-rGO/GDL cathode where rGO is reduced graphene oxide and GDL stands for gas diffusion layer. The selection of Ir was because it is one of the best-known fuel cell ORR catalysts. Indeed, the Li-O_2 cell ran well with a low polarization gap of 0.9 V. It was found that $LiIr_3$ formed on the surface of Ir nanoparticles. The discharge product was exclusively LiO_2 based on various experimental techniques.[7] Density functional calculations indicated a lattice match of LiO_2 on $LiIr_3$ surfaces suggesting epitaxial-like growth.

Following these findings, a cathode based on 1.5 nm Ir nanoparticles on rGO was used.[8] Upon use in a Li-O_2 cell the nanoparticles evolved into larger ones of about 5 nm. The formation of an $LiIr_3$ outer shell on the Ir nanoparticles was observed *ex-situ* after operation of the Li-O_2 cell. In addition, a very thin layer (~2 nm) of LiO_2 over $LiIr_3$ was observed with use of TEM after discharge. DFT calculations indicated the following reaction could occur on the surface of Ir nanoparticles that explains the formation of the $LiIr_3$ outer shell:

$$LiO_2(s) + 3\ Ir(s) \rightarrow LiIr_3(s) + O_2(g) \qquad (1)$$

Interestingly, the formation energy for Equation (1) is -5.90 eV, a very favorable and exothermic condition.[8]

In another study a Li-O_2 battery was based on $LiIr_3$ that had been synthesized in bulk quantity. In contrast to the formation of $LiIr_3$ *in-situ* under electrochemical condition at ambient temperature,[8] the bulk synthesis of $LiIr_3$ requires 800°C over eight days.[9] Initially the dramatically different synthesis conditions of thermal heating vs. electrochemical room temperature formation were puzzling. However, the LiO_2 apparently plays a crucial role in assisting the formation of $LiIr_3$ as indicated in Eq 1 in the case of Ir nanoparticles. The strategy of using $LiIr_3$-rGO/GDL as a cathode leads to large LiO_2 nanoparticles with diameters larger than 200 nm. In addition, this is the first time that a TEM image of a LiO_2 aggregate was successfully captured under 80 KV scanning electron beam irradiation while 200 KV irradiation led to decomposition from LiO_2 to Li_2O.[10] Also another LiIr alloy, LiIr-rGO/GDL, was explored as a cathode in a Li-O_2 cell. The cell ran well with a low over-potential gap of 0.8 V (3.50 – 2.75 V) and reached 100 cycles at 1000 mAh/g capacity with replacement of the Li anode. In addition, DFT calculations revealed that the LiO_2 (111) has a lattice match with LiIr (111) and LiO_2 (101) with LiIr (110). [11]

In this paper a simple goodness of fit R factor to gauge how well a template surface structure can support LiO_2 growth such as found for IrLi and Ir_3Li is developed. The R factor is a quantitative measurement to calculate the geometric difference in the unit cells of specific Miller Index 2D planes of the matching template molecule and LiO_2. Using this as a guide, the R factors for $LiIr_3$, LiIr, and $La_2NiO_{4+\delta}$, are found to be good. The guide is attested by simple extension to other noble metal intermetallics with initial electrochemical cycling data including $LiRh_3$, LiRh, and Li_2Pd. Finally, the template concept is further extended to main group elements.

Experimental

The following ICSD standard/reported structures are used for visualization and epitaxy analysis with VESTA software. The LiO_2 (ICSD-180561) that is from calculations, all structures are reported experimental data: $LiIr_3$ ICSD-104488, LiIr ICSD-104487, $La_2NiO_{4+\delta}$ ICSD-69172, $LiRh_3$ ICSD-642290, LiRh ICSD-150551, Li_2Pd ICSD-104773, and Li_2Ca ICSD-413207. VESTA (Visualization for Electronic and STructural Analysis) Ver. 3.5.8 is used for visualization of the template and lithium superoxide epitaxial interfaces.[16]

Raman spectroscopy (Renishaw inVia) was performed using a HeNe laser with a wavelength of 633 nm. 10% of the maximum 13 mW laser power was used, and spectrum collection was set up in a 180 ° reflective mode with a time constant of 200 s. Scanning electron microscopy (SEM; Hitachi S-4700) coupled with EDAX (energy dispersive X-ray analysis) is used throughout. Sample SPPd6 (Fig. 6) is Pd-Super P carbon/GDL cathode that is prepared with thermally evaporated (Edwards Auto 360) Pd film with 6 nm thickness over Super P carbon that is coated over a porous Gas Diffusion Layer.

A Swagelok cell in a glass chamber was used for Li-O_2 battery testing. A 1 M Li triflate salt in tetraethyleneglycol dimethyl ether (TEGDME) was used as the Li-O_2 cell electrolyte with 100 mA/g current density and 500 mAh/g capacity. Electrochemical cycling was carried out using a MACCOR® S4000 cycler at 24 °C.

Results and Discussion

Growth of LiO_2 over $LiIr_3$

Although the formation energy of LiO_2 is predicted to be -1.04 eV/atom, LiO_2 is unstable with respect to disproportionation to Li_2O_2 at ambient conditions. [5, 12, 13] In the early literature, LiO_2 has only been reported to be isolated at 10 K with use of solid N_2 matrix.[14] Recently, we demonstrated the presence of LiO_2 in a Li-O_2 battery by matching its electron diffraction with the calculated structure.[15] This battery was based on Ir nanoparticles as the cathode and it was discovered that $LiIr_3$ formed in the cell supported the growth of LiO_2.[7] Since $LiIr_3$ favors the formation of LiO_2, in another paper we prepared $LiIr_3$ in bulk through high temperature solid state synthesis.[10] The most intense XRD peak of the high temperature synthesized $LiIr_3$ is the (121) peak. In the presence of the $LiIr_3$ cathode, LiO_2 apparently forms exclusively as the discharge product through a "template assisted LiO_2 growth process". The LiO_2 (111) plane is believed to be stabilized through a lattice matching interface with $LiIr_3$ (121).[7] Here VESTA (Visualization for Electronic and STructural Analysis) software [16] was used to visualize a LiO_2 (111) plane together with a $LiIr_3$ (121) plane (Figures 1a and 1b, respectively) to show the matching interfacial layers. The templated LiO_2 growth suppresses self-disproportionation to form Li_2O_2 and O_2. A kinetics study has shown that LiO_2 can undergo a first order disproportionation reaction during the discharge process without a template support.[13]

1a **1b**

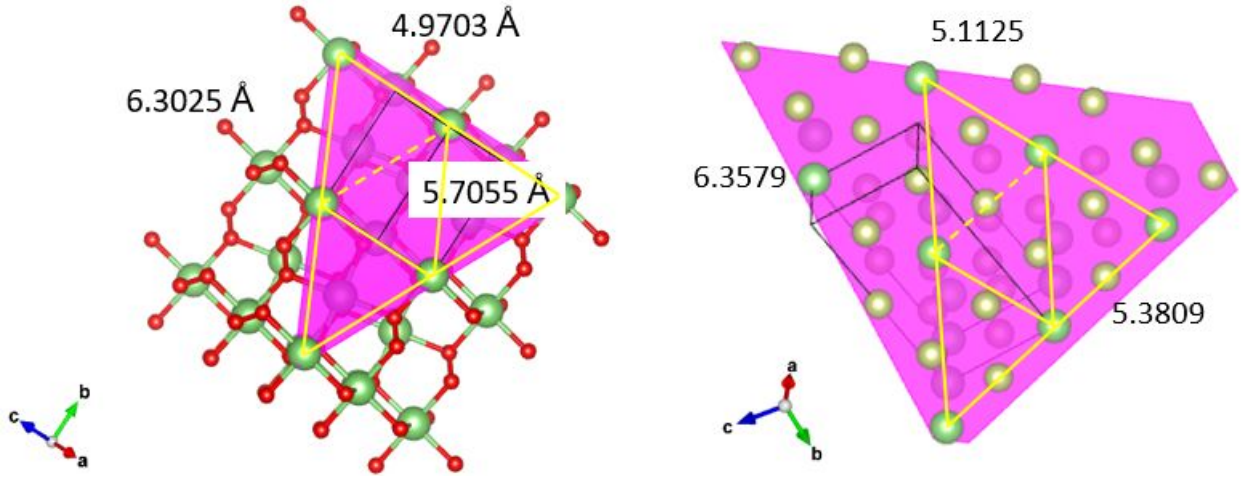

Fig. 1a LiO_2 (111) plane shown in pink with an in-plane rhombus unit cell marked in yellow. Li: green and O: red. (LiO_2 ICSD-180561) Fig. 1b $LiIr_3$ (121) plane with a similar in-plane rhombus unit cell marked in yellow. Li: green and Ir: gold. ($LiIr_3$ ICSD-104488)

We speculate that the intermetallic $LiIr_3$ may act as a template for growth of the crystalline LiO_2, as has been found in template-controlled nucleation and growth of other crystalline materials.[17] DFT calculations on the interface between LiO_2 and Ir_3Li, found that some crystalline faces had good lattice matches (Ref [7], Supplementary Fig. S13), as would be required for stabilization of crystalline LiO_2.

For another Ir containing catalyst, LiIr, the LiIr-rGO/GDL cathode also cycled well.[11] Both LiO_2 (101) over LiIr (110) (Figure 2a and 2b, respectively) and LiO_2 (111) (as shown in Figure 1a) over LiIr (111) (Figure 3) were shown to have good lattice matches through DFT calculations.[11] Since good lattice matching interfaces between LiO_2 and LiM_x play a crucial role in supporting LiO_2 deposition and lower the charging over-potential, we decided to develop a way to estimate how well a potential cathode material matches the lattices of the LiO_2 surfaces, which is described in this paper.

Goodness of Fit R factor

A simple model is developed to quantitatively estimate how well the lattice of a LiM_x layer matches that of LiO_2. A rhombus unit cell is chosen for the 2D LiO_2 (111) plane as indicated in Figure 1a. The individual R_n (n = 1 - 3) factors (Equation 3) measure the difference of each unit cell length in Å over the unit cell length of LiO_2. The goodness of the fit R factor (Equation 4) combines the contribution from all three sides and represents how well the LiM_x layer fits that of LiO_2. For example, the two sides and short diagonal lengths (dash line) of the unit cell for LiO_2 (111) plane are: l_1 6.302 Å, l_2 5.705 Å, and l_3 4.970 Å, based on ICSD-180561 of a calculated LiO_2 structure. The equivalent experimental lengths for $LiIr_3$ (121) plane are: l_1' 6.358 Å, l_2' 5.381 Å, and l_3' 5.113 Å, respectively, (ICSD-104488, Figure 1b).

$$R_n = \frac{l_n - l'_n}{l_n}, \; n = 1 - 3 \qquad (3)$$

$$R = \sqrt{(R_1^2 + R_2^2 + R_3^2)} = 6.43\% \qquad (4)$$

The lower the value of the goodness of fit (R) the better and the R value for LiO_2 (111) plane over the $LiIr_3$ (121) plane is 6.4%. We also estimate the R factor for the LiO_2 (101) plane over LiIr (110) plane to be 15.2% and LiO_2 (111) over LiIr (111) to be 22.4%, respectively. A non-lithium containing metal oxide ternary compound, $La_2NiO_{4+\delta}$, has been reported that stabilizes growth of LiO_2 layer on the terminating surface of the Ni oxide (001) layer.[18] The $La_2NiO_{4+\delta}$ (001) plane (pink) is shown in Figure 4. The four corners of the yellow box in Figure 4 indicate lithium sites reported in reference 18 through a DFT calculation. Since experimental evidence based on a Raman peak at 1123 cm^{-1} together with a low charge overpotential ~3.8 V were observed [18] that are indicative of the presence of LiO_2, its R factor can be estimated with use of the $La_2NiO_{4+\delta}$ unit cell length (a = b = 3.869 Å). The calculation details are in Table 1. The goodness of fit R for LiO_2 (101) (Figure 2a) over $La_2NiO_{4+\delta}$ (001) through a "Li-rich surface" is estimated to be 37.1%.

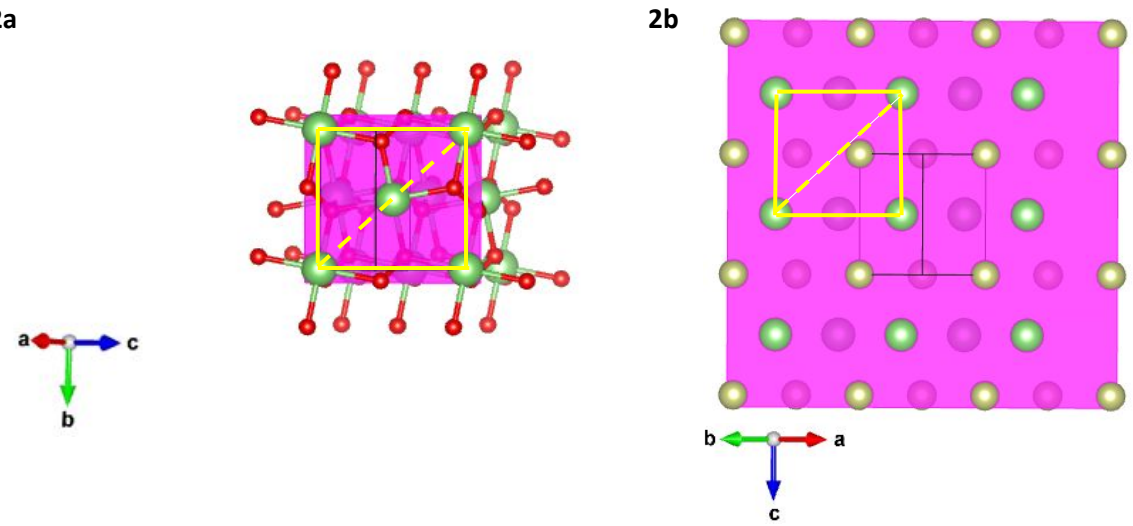

Fig. 2a LiO_2 (101) plane shown in pink with a nearly square unit cell marked in yellow. Li: green and O: red. (LiO_2 ICSD-180561) Fig. 2b LiIr (110) plane also with a nearly square unit cell marked in yellow. Li: green and Ir: gold. (LiIr ICSD-104487)

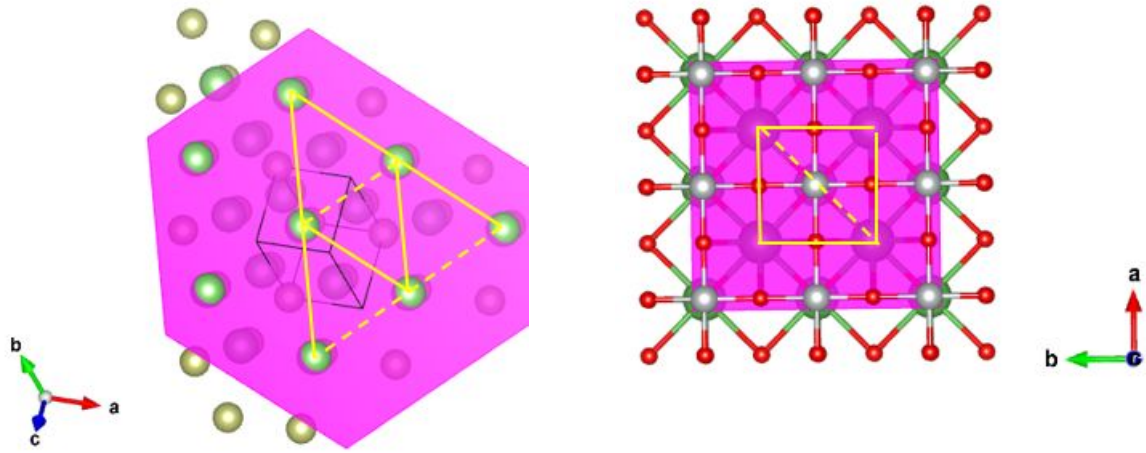

Fig. 3 (Left) LiIr (111) plane in pink with an in-plane rhombus unit cell that supports epitaxial growth of LiO_2 (111) Fig. 1a.
Fig. 4 (Right) $La_2NiO_{4+\delta}$ (001) plane in pink showing four unit cells. Ni is the small gray atom and O is red. The four corners of the yellow box indicate proposed Li atom deposition sites that leads to LiO_2 layer growth. [18] ($La_2NiO_{4+\delta}$ from ICSD-69172, I4/mmm a = b = 3.869Å)

Application of R Factor and Search for New Templates

A simple application of the R factor is to check/verify LiM_x surface with other elements in the same column of the periodic table for LiO_2 stabilization. Since both $LiRh_3$ and LiRh are isostructural to $LiIr_3$ and LiIr, respectively, [19] their R factors were calculated. For LiO_2 (111) over $LiRh_3$ (121), LiO_2 (101) over LiRh (110), and LiO_2 (111) over LiRh (111), they are 6.3%, 16.0%, and 23.1%, respectively. (Table 1) These

values are very similar to that of the corresponding $LiIr_x$ intermetallics. In an experimental study we treated $RhCl_3$ with hydrazine and prepared Rh-rGO/GDL cathode for a Li-O_2 cell. The characterization of the cathode reveals a Rh peak in EDAX. The discharge product has Raman scattering peaks at 1125 and 1500 cm^{-1}, and a low charging plateau ~ 3.6 V between the 5th and 30th electrochemical cycles.[20] These results indicate that $LiRh_3$ and LiRh are very likely to have the same template assisted LiO_2 stabilization effect.

Table 1 Goodness of fit R factor calculations for LiO_2 over $LiIr_3$, LiIr, $La_2NiO_{4+\delta}$, $LiRh_3$, and LiRh

LiO_2 (hkl)/LiM_x(hkl)	R_1	R_2	R_3	R
LiO_2 (111) Li-Li	4.970	5.705	6.302	
$LiIr_3$ (121) Li-Li	5.113	5.381	6.358	
Δ Difference	-0.143	0.324	-0.056	
Δ / LiO_2 Li-Li	-0.0288	0.0568	-0.00889	R = 6.43%
LiO_2 (101)	4.877	4.970	6.963	
LiIr (110)	4.397	4.588	6.355	
Δ / LiO_2	0.09842	0.07686	0.08732	R = 15.2%
LiO_2 (111)	4.970	5.705	6.302	
LiIr (111)	4.588	5.133	5.133	
Δ / LiO_2	0.0769	0.1003	0.1855	R = 22.4%
LiO_2 (101)	4.877	4.970	6.963	
$La_2NiO_{4+\delta}$ (001)	3.869	3.869	5.472	
Δ Difference	1.008	1.101	1.491	
Δ / LiO2	0.2067	0.2215	0.2141	R = 37.1%
LiO_2 (111)	4.970	5.705	6.302	
$LiRh_3$ (121)	5.068	5.362	6.311	
Δ/LiO_2	-0.0197	0.0601	-0.00143	R = 6.3%
LiO_2 (101)	4.877	4.970	6.963	
LiRh (110)	4.359	4.588	6.329	
Δ/LiO2 Li-Li	0.1062	0.0769	0.0911	R = 16.0%
LiO_2 (111)	4.970	5.705	6.302	
LiRh (111)	4.588	5.101	5.101	
Δ / LiO_2	0.0769	0.1059	0.1906	R = 23.1%

Among the noble metal catalysts, Pd on a carbon support is of interest since Pd is among the best fuel cell catalysts for ORR. The potential for Li intercalation into Pd like that of $LiIr_3$ formation (Equation 1) during cycling led us to explore the Li-Pd binary system. Based on the Li-Pd phase diagram, there is only one congruent line compound, Li_2Pd. [21] A line compound is a preferred candidate for template assisted LiO_2 growth due to its well-defined stoichiometry and well-ordered structure. The thermal formation condition for Li_2Pd is reported to be 800 °C for 1 hr. [22] Potential lattice matching between

LiO_2 and different facets of Li_2Pd was investigated. Shown in Figure 5a is the Li_2Pd (100) facet in pink that is associated with the strongest XRD peak and LiO_2 (011) and (110) planes are shown in Figure 5b and 5c, respectively. The calculated R factors for LiO_2 (011) over Li_2Pd (100), LiO_2 (110) over Li_2Pd (100), and LiO_2 (111) (Figure 1a) over Li_2Pd (101) (Figure 5d) are 7.39%, 7.39%, and 27.6%, respectively. These R factors are within the range of forming stable LiO_2-Li_2Pd interfacial layers compared to that of LiO_2 over $LiIr_3$, LiIr and $La_2NiO_{4+\delta}$. The first 20 cycles of electrochemical cycling of a Li-O_2 cell with a Pd/carbon/GDL cathode is shown in Figure 6a. Other than the first cycle, the low overpotential of 0.7 V (2.7–3.4 V), Pd signal from EDAX, and a Raman scattering peak at ~1145 cm^{-1} (Figure 6b) indicate the presence of LiO_2.[23] The Raman peak is higher than the typical value of 1125 cm^{-1} [15, 24] but not too far from a reported 1137 cm^{-1} [12] in one study for the O-O stretch. Therefore, these results also support template assisted LiO_2 growth on Li_2Pd.

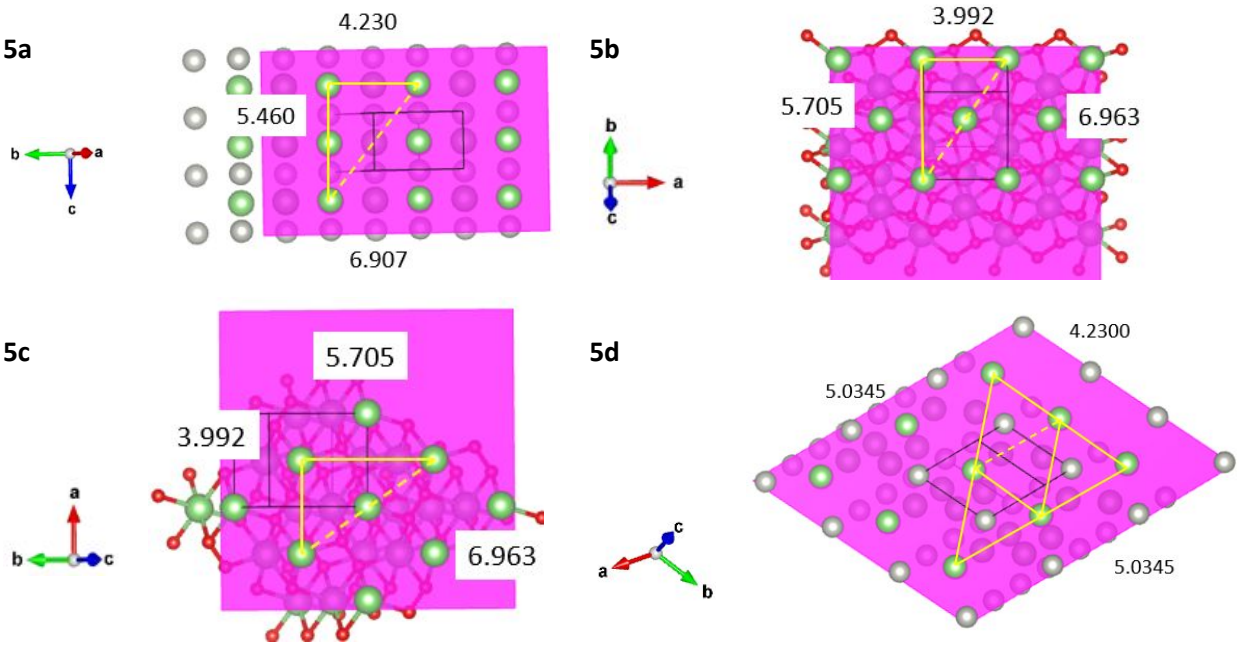

Fig. 5a Li_2Pd (100) plane in pink. The two sides of a rectangular unit cell and diagonal (dash line) are marked in yellow. (Li_2Pd ICSD-104773) Fig. 5b LiO_2 (011) plane in pink. The two sides and diagonal (dash line) of a 2D unit cell of the plane are marked in yellow. (LiO_2 ICSD-180561) Fig. 5c LiO_2 (110) plane in pink. The two sides and diagonal (dash line) of a 2D unit cell of the plane are marked in yellow. Fig. 5d The Li_2Pd (101) plane to support LiO_2 (111) (Figure 1a) in pink. A rhombus 2D unit cell for the plane is marked in yellow.

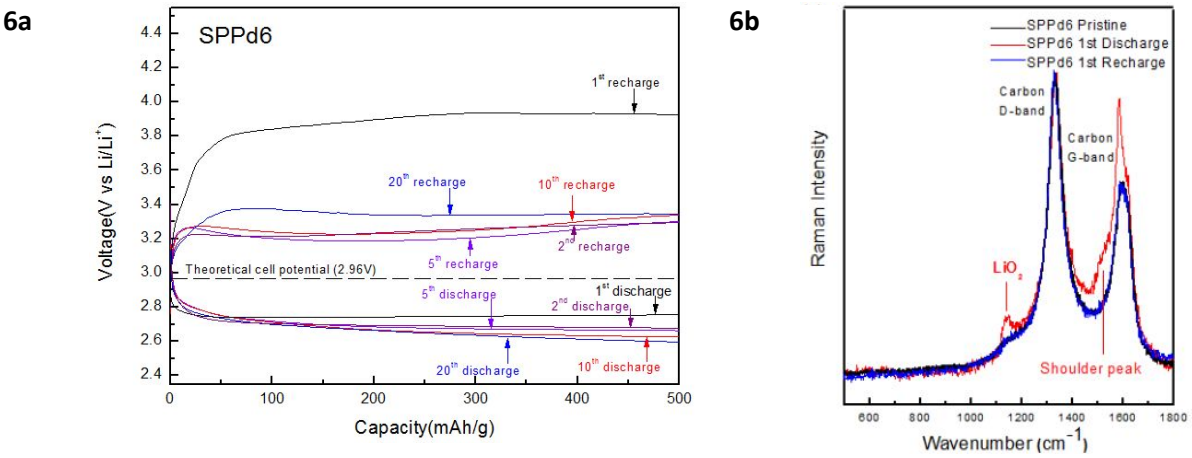

Fig. 6a Pd (6 nm thick) was thermally evaporated over carbon (Super P) to make a SPPd6/GDL cathode. The EC cycling for the first 20 cycles at 100 mA/g current density and 500 mAh/g capacity shows a low overpotential of 0.7 V. Fig. 6b Raman spectra of SPPd6 pristine (black), 1st discharge (red), and 1st charge (blue). LiO_2 peak at 1145 cm^{-1} is shown after the first discharge.

Main Group LiM_x Template

Since one consideration as to whether template assisted LiO_2 growth is possible depends on geometric requirements, the search for desirable templates can also be extended to main group LiM_x templates. The first element in the main group we considered was magnesium. However, the Li-Mg binary phase diagram does not contain any line compounds. This can be understood through the Hume-Rothery Rule for complete miscibility since the atomic radii of Li (167 pm) and Mg (145 pm) are within 15% (or 167± 25 pm). [25] The Li and Mg atoms in a solid solution will be entirely random and not suitable for our template application.

The next element is Ca (194 pm) and the Li-Ca phase diagram indicates only one line compound, Li_2Ca. [26] The XRD (x-ray diffraction) pattern of Li_2Ca (ICSD-413207 Cubic) reveals three prominent peaks for (111), (220 and $20\bar{2}$), and (311 and $3\bar{1}\ \bar{1}$). A potential lattice match with LiO_2 for all five different facets was explored and all five matches at different R values. Since the (311) and ($3\bar{1}\ \bar{1}$) as well as (220) and ($20\ \bar{2}$) are in the same family of planes, respectively, only Li_2Ca (111), (311), and ($20\bar{2}$) are shown in Figures 7a-c. The calculated R factors for LiO_2 (111) over Li_2Ca (111), Li_2Ca (311) and Li_2Ca ($20\bar{2}$) are 25.7%, 14.7%, and 10.1%, respectively. All three R values are within a possible LiO_2/Li_2Ca lattice match range and suggest that Li_2Ca (cubic) would be a good candidate for template assisted LiO_2 growth.

7a

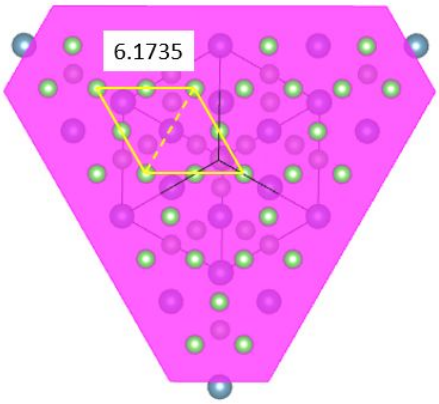

Fig. 7a Li_2Ca (111) plane in pink with a rhombus unit cell formed by two equilateral triangles marked in yellow. (Li_2Ca ICSD-413207)

7b

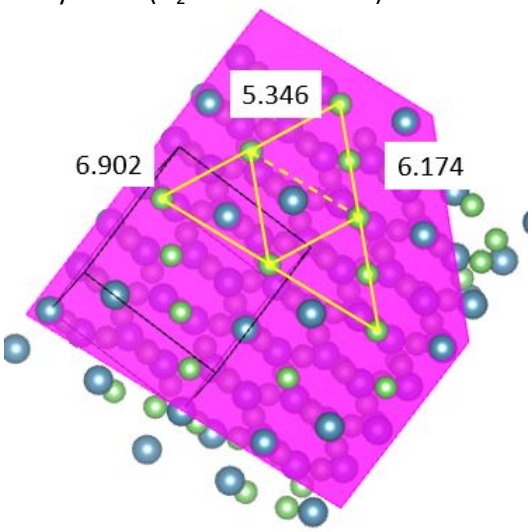

7c

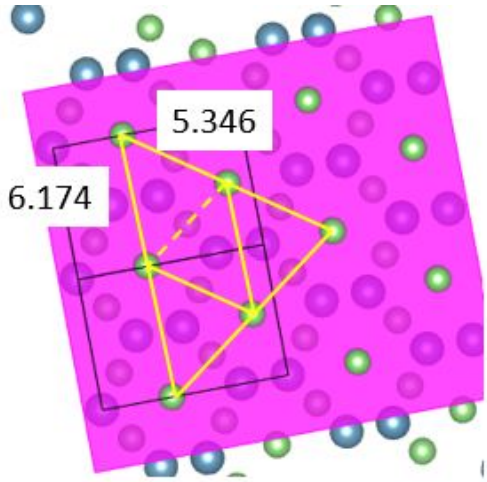

Fig. 7b Li_2Ca (311) plane in pink with a rhombus unit cell for the 2D (311) plane marked in yellow.
Fig. 7c Li_2Ca ($20\bar{2}$) plane in pink with a rhombus unit cell consists of two isosceles triangles marked in yellow.

Table 2 Goodness of fit R factor calculations for LiO_2 over Li_2Pd and Li_2Ca

LiO_2 (hkl)/LiM_x(hkl)	R_1	R_2	R_3	R
LiO_2 (111) Li-Li Å	4.970	5.705	6.302	
Li_2Pd (101) Li-Li	4.2300	5.0345	5.0345	
Δ Difference	0.740	0.671	1.268	
Δ / LiO_2 Li-Li	0.1489	0.1175	0.201	27.6%
LiO_2 (011)	3.992	5.705	6.963	
Li_2Pd (100)	4.230	5.460	6.907	

Δ / LiO_2	-0.05962	0.04294	0.008043	7.39%
LiO_2 (111) Li-Li	4.970	5.705	6.302	
Li_2Ca (111) Li-Li	6.174	6.174	6.174	
Δ Difference	-1.204	-0.469	0.128	
Δ / LiO_2 Li-Li	-0.2423	-0.08221	0.0203	25.66%
LiO_2 (111) Li-Li	4.970	5.705	6.302	
Li_2Ca (311)	5.346	6.174	6.902	
Δ / LiO_2	-0.0757	-0.0822	-0.0952	14.68%
LiO_2 (111) Li-Li	4.970	5.705	6.302	
Li_2Ca ($20\bar{2}$)	5.346	5.346	6.174	
Δ / LiO_2	-0.0757	0.0629	0.0203	10.05%

Conclusions

In this paper, based on our recent work on the development of cathode materials for aprotic lithium oxygen batteries including two intermetallic compounds, $LiIr_3$ and LiIr, that likely form epitaxy-like interfaces with LiO_2, together with a literature $La_2NiO_{4+\delta}$ metal oxide that also triggers the growth of LiO_2 lead us to the concept that this template assisted LiO_2 growth helps to stabilize the LiO_2 discharge product in a Li-O_2 battery and contributes to a low charging overpotential. A simple goodness of fit R factor was developed to gauge how well a template can support LiO_2 growth with use of these known cathode materials as the reference points. Guidelines for developing new template assisted materials that support LiO_2 epitaxial growth are listed below:

1) A good LiM_x template where M is a transition or main group metal must be electronically conductive.
2) A LiM_x template with a well-defined structure and stoichiometry is preferred as disorder will likely hinder the template mechanism. The 2D unit cell of the LiM_x plane must have the same symmetry as one of the LiO_2 planes. The (110), (011), (101), and (111) planes of LiO_2 are the most predominant ones based on the ICSD calculated structure.
3) The goodness of fit R factor can be used as a guide to search for possible LiO_2 growth template. While the highest R factor found was for $La_2NiO_{4+\delta}$ at 37%, the R factor for new template/catalyst follows the lower the better rule. R factor less than 22% is expected to work well as demonstrated by $LiIr_3$ (R = 6.4%) and LiIr (R = 15.2 – 22.4%).
4) An R factor larger than 37% may still be considered only if the new LiM_x templates can withstand compression or tension.

Toward lowering the overpotential gap, the template assisted LiO_2 growth strategy is quite promising. Once the charging potential is lower than 4 V (vs Li/Li^+), side reactions due to electrolyte decomposition can be reduced. To have long cycle stability, the Li metal anode needs to be protected. Choosing a compatible Li protection route together with template assisted LiO_2 growth, if successful, will help advance Li-O_2 energy storage development.

Author Contributions

All Authors contributed equally to this manuscript.

Conflicts of interest statement

There are no conflicts to declare.

Acknowledgements

This work was supported by the U.S. Department of Energy under Contract No. DE-AC02-06CH11357 from the Vehicle Technologies Office, Office of Energy Efficiency and Renewable Energy. VESTA (Visualization for Electronic and STructural Analysis) Ver. 3.5.8 is used for visualization of the template and lithium superoxide epitaxial interfaces.[16]

References

1. H. Kitaura and H. Zhou, Scientific Reports 2015, 5:13271, DOI: 10.1038/srep13271
2. J.S. Hummelshøj, J. Blomqvist, S. Datta, T. Vegge, J. Rossmeisl, K.S. Thygesen, A.C. Luntz, K.W. Jacobsen and J.K. Nørskov, J. Chem. Phys. 2010, 132, 071101.
3. K.C. Lau, L.A. Curtiss and J. Greeley, J. Phys. Chem. C 2011, 115, 23625–23633.
4. M.D. Radin, J.F. Rodriguez, F. Tian and D.J. Siegel, J. Am. Chem. Soc. 2012, 134, 1093−1103.
5. Materials Project LiO_2 mp-1018789, https://next-gen.materialsproject.org/materials/mp-1018789?chemsys=Li-O
6. N.R. Mathiesen, S. Yang, J.M. García-Lastra, T. Vegge and D.J. Siegel, Chem. Mater. 2019, 31, 9156−9167.
7. J. Lu, Y.J. Lee, X. Luo, K.C. Lau, M. Asadi, H.-H. Wang, S. Brombosz, J. Wen, D. Zhai, Z. Chen, D.J. Miller, Y. S. Jeong, J.-B. Park, Z.Z. Fang, B. Kumar, A. Salehi-Khojin, Y.-K. Sun, L.A. Curtiss and K. Amine, Nature 2016, 529, 377.
8. A. Halder, A.T. Ngo, X. Luo, H.-H. Wang, J.G. Wen, Pe. Abbasi, M. Asadi, C. Zhang, D. Miller, D. Zhang, J. Lu, P.C. Redfern, K.C. Lau, R. Amine, R.S. Assary, Y.J. Lee, A. Salehi-Khojin, S. Vajda, K. Amine and L.A. Curtiss, J. Phys. Chem. A 2019, 123, 10047−10056.
9. H.C. Donkersloot, J.H.N. Van Vucht, The Crystal Structure of IrLi, Ir_3Li and $LiRh_3$, J. Less-Common Met. 1976, 50, 279−282.
10. S.T. Plunkett, C. Zhang, K.C. Lau, M.R. Kephart, J.G. Wen, D.Y. Chung, D. Phelan, Y. Ren, K. Amine, S. Al-Hallaj, B.P. Chaplin, H.-H. Wang and L.A. Curtiss, Nano Energy 2021, 90, 106549.
11. S.T. Plunkett, A. Kondori, D.Y. Chung, J. Wen, M. Wolfman, S.H. Lapidus, Y. Ren, R. Amine, K. Amine, A.U. Mane, M. Asadi, S. Al-Hallaj, B.P. Chaplin, K.C. Lau, H.-H. Wang and Larry A. Curtiss, ACS Energy Lett. 2022, 7, 2619−2626.
12. Z. Peng, S.A. Freunberger, L.J. Hardwick, Y. Chen, V. Giordani, F. Bardé, P. Novák, D. Graham, J.-M. Tarascon, and P.G. Bruce, Angew. Chem. Int. Ed. 2011, 50, 6351 –6355.

13. D. Zhai, H.-H. Wang, J. Yang, K.C. Lau, K. Li, K. Amine and L.A. Curtiss, J. Am. Chem. Soc. 2013, 135, 15364−15372.
14. D.M. Lindsay and D.A. Garland, J Phys. Chem. 1987, 91, 6158-6161.
15. D. Zhai, K.C. Lau, H.-H. Wang, J. Wen, D.J. Miller, J. Lu, F. Kang, B. Li, W. Yang, J. Gao, E. Indacochea, L.A. Curtiss and K. Amine, Nano Lett. 2015, 15, 1041−1046.
16. K. Momma and F. Izumi, "VESTA 3 for three-dimensional visualization of crystal, volumetric and morphology data," J. Appl. Crystallogr., 2011, 44, 1272-1276.
17. E.M. Pouget, P.H.H. Bomans, J.A.C.M. Goos, P.M. Frederik, G. de With, N.A.J.M. Sommerdijk, Science 2009, 323, 1455-1458.
18. S. Samira, S. Deshpande, C.A. Roberts, A.M. Nacy, J. Kubal, K. Matesić, O. Oesterling, J. Greeley and E. Nikolla, Chem. Mater. 2019, 31, 7300−7310.
19. J. Sangster and A.D. Pelton, Journal of Phase Equilibria 1991, 12, 6, 682-684.
20. C. Zhang, CME (Civil, Mater. and Enviro. Eng.), UIC Master Thesis 2017.
21. J. Sangster and A.D. Pelton, Journal of Phase Equilibria 1992, 13, 1, 63-66.
22. J.H.N. Van Vucht and K.H.J. Buschow, J. of the Less-Common Metals, 1976, 48, 345 – 347.
23. J. Gao, CME (Civil, Mater. and Enviro. Eng.), UIC PhD Thesis 2015.
24. D. Zhai, H.-H. Wang, K.C. Lau, J. Gao, P.C. Redfern, F. Kang, B. Li, E. Indacochea, U. Das, H.-H. Sun, H.-J. Sun, K. Amine and L.A. Curtiss, J. Phys. Chem. Lett. 2014, 5, 2705−2710.
25. J.F. Shackelford, Introduction to Materials Science for Engineers, 2015 Pearson plc, London, UK.
26. C.W. Bale and A.D. Pelton, Bulletin of Alloy Phase Diagrams 1987, 8, 2, 125-127.